Dovepress

ORIGINAL RESEARCH

Tumor ablation using novel photothermal Na$_x$WO$_3$ nanoparticles against breast cancer osteolytic bone metastasis

Shuo Jie
Xiaoning Guo
Zhengxiao Ouyang [ID]

Department of Orthopedics, The Second Xiangya Hospital, Central South University, Changsha, Hunan 410011, People's Republic of China

Backgrounds: Profiting from the development of nanomaterials, photothermal therapy (PTT) has been discovered as efficient tumor ablation strategy for breast cancer.

Materials and methods: Novel oxygen vacancy-rich tungsten bronze nanoparticles (Na$_x$WO$_3$) were synthesized through a simple pyrogenic decomposition process. TEM, XRD, UV-vis-NIR, photothermal conversion ability, and photothermal stability were performed. The viabilities of 293T and 4T1 cells after treating with 200 μg/mL Na$_x$WO$_3$ nanoparticles for 24 or 48 hrs were both above 80%, which proved the good biosafety and cytotoxicity of Na$_x$WO$_3$ in vitro. Two in vivo breast cancer models, namely percutaneous and intratibial 4T1 models were established and Na$_x$WO$_3$ (20 mg/kg) with power intensity of 1.5 W/cm^2 980 nm laser photothermal treatment was used in vivo.

Results: We successfully synthesized ~150 nm Na$_x$WO$_3$ nanoparticles with desirable PTT effects, as evidenced by the temperature increase from 25.8°C to 41.8°C in 5 mins under the irradiation of 980 nm laser (1 mg/mL). Also, cellular compatibility of Na$_x$WO$_3$ nanoparticles was found upon physiologic 293T cells, in contrast with significant cytotoxicity against breast cancer 4T1 cell in vitro dose-dependently. Besides, two in vivo breast cancer models showed the decent tumor ablation ability of Na$_x$WO$_3$ nanoparticles, demonstrating percutaneous 4T1 tumor elimination without recurrence during 2 weeks observation as well as intratibial breast cancer inhibition with decreased bone destruction and tumor volume after Na$_x$WO$_3$+PTT in vivo.

Conclusion: For the first time, we developed a novel oxygen vacancy-rich tungsten bronze nanoparticles (Na$_x$WO$_3$) through a simple pyrogenic decomposition process for PTT. Both in vitro and in vivo experiments showed the good PTT ability and tumor ablation effects of synthesized Na$_x$WO$_3$ nanoparticles against breast cancer osteolytic bone metastasis. Additionally, our oxygen-deficient Na$_x$WO$_3$ nanoparticles will expand the research horizons of PTT nanomaterials.

Keywords: oxygen vacancy, Na$_x$WO$_3$ nanoparticles, photothermal therapy, breast cancer bone metastasis

Correspondence: Xiaoning Guo;
Zhengxiao Ouyang
Department of Orthopedics, The Second Xiangya Hospital, Central South University, No.139 Renmin Road, Changsha, Hunan 410011, People's Republic of China
Tel +86 7 318 529 5127;
+86 1 354 856 0675
Email guoxiaoning@csu.edu.cn;
ouyangzhengxiao@csu.edu.cn

Introduction

Breast cancer is the second leading cause of cancer-related deaths among women worldwide,[1] and is also the most common cancer among Chinese women.[2] Osteolytic bone metastasis accounts for approximately 80% of patients with advanced-stage breast cancer,[3] which inevitably results in skeletal morbidity, including pathological fractures, hypercalcemia and neurological compression.[4] Currently, conventional treatment for bone metastasis of breast cancer such as chemotherapy is limited by its high toxicity

and drug resistance.[5] Removal of tumors by surgery is not suitable for small, poorly defined foci. Based on the generally osteolytic nature of the lesion induced by breast cancer, bisphosphonates and denosumab have become classic medications, however, bisphosphonates still have serious adverse effects such as osteonecrosis of the jaw and subtrochanteric fractures. Denosumab was reported to increase the risk of pancreatitis and endocarditis, erysipelas and infectious arthritis.[6,7] Newly reported drugs such as Cathepsin K inhibitor odanacatib have been withdrawn from the clinical trials for safety reasons.[8] Other treatments such as c-Src inhibitor are still in clinical trials to date.[8] Hence, novel safe and efficient therapies in the treatment of breast cancer bone metastasis are needed.

Nowadays, approaches of nanomedicine have gained increasingly number of attention[9,10] in the treatment of intractable cancers, especially breast cancer metastasis. Profiting from the discovery of enhanced permeability and retention (EPR) effect and the development of nanotechnology, photothermal therapy (PTT) has been widely developed by researchers. PTT based on near-infrared (NIR) radiation is a promising alternative or supplement to traditional cancer therapy.[11,12] For instance, gold nanoparticles,[13–21] transition-metal chalcogenides,[22–24] and carbon-based nanostructures[25,26] have been explored as photothermal agents because of their effective photothermal conversion ability. Recently, oxygen vacancy-rich transition-metal oxides are particularly appealing for PTT due to their metallic features and strong surface plasmon resonance (SPR) effect.[27–29] Also, non-stoichiometric MoO_{3-x} nanosheets showed efficient tumor homing capabilities and effective tumor ablation ability due to their strong localized-SPR effects in the NIR region.[30]

In this study, for the first time, we developed a novel oxygen vacancy-rich tungsten bronze nanoparticles (Na_xWO_3) through a simple pyrogenic decomposition process for PTT. Deep blue Na_xWO_3 nanoparticles show strong absorbance in NIR region (980 nm), which enable the deeper penetration into bone tissue than common 808 nm laser that is significant for the treatment against cancer bone metastasis to eradicate tumor cells. Under the irradiation of NIR laser upon Na_xWO_3, obvious temperature increase was observed derived from excellent photothermal conversion ability of Na_xWO_3 nanoparticles. Therefore, our efficient PTT strategy of Na_xWO_3 could provide brand-new insight into future cancer bone metastasis treatment clinically, which also expand the research horizons of PTT nanomaterials.

Materials and methods
Materials
Dimethyl sulfoxide and 1-octadecene (90%) were purchased from Sinopharm Group (Sinopharm, Hongkong, China). Oleic acid and cyclohexane (C_6H_{12}) were obtained from Adamas-beta Company (Adamas-beta, Shanghai, China). Sodium tungstate dehydrate ($Na_2WO_4 \cdot 2H_2O$) was purchased from Sigma-Aldrich (St Louis, MO, USA). All chemical reagents were used as bought without any purification. All aqueous solution used in the experiment was deionized water (18.2 MΩ.cm) obtained from Milli-Q water purification system.

Synthesis of Na_xWO_3 nanoparticles
In a typical synthesis of Na_xWO_3 nanorods, 10 mL of oleic acid and 30 mL of 1-octadecene and placed into a 100 mL flask, after that, 5 mL of ammonia solution with 2 mmol of $Na_2WO_4 \cdot 2H_2O$ was added into the flask drop wisely with magnetic stirring. After sufficient stir, the mixed solution was heated to 80°C under argon environment so as to evaporate ammonia. After the evaporation, the solution was heated to 280°C and maintained for 1 hr and then cooled to room temperature. Finally, the deep blue solution was centrifuged (13,000 rpm, 10 mins), the blue precipitate was re-dispersed in 10 mL of cyclohexane and 5 mL of ethanol-mixed solution and was centrifuged (13,000 rpm, 10 mins) to scour off the surface oleic acid. The final product was re-dispersed in 30 mL of deionized water for further use.

Materials characterization
Size and morphology of Na_xWO_3 nanoparticles were investigated using transmission electron microscopy (TEM) (JEOL 200CX, Tokyo,Japan). X-ray diffraction (XRD) was measured on a Rigaku D/MAX-2250 V at Cu Kα (λ=0.154056 nm) with a scanning rate of $4°min^{-1}$ in the 2θ range of 10°–80°. Photothermal performance of Na_xWO_3 nanoparticles was monitored by a photothermal camera (FLIRTM A325SC camera, Wilsonville, Oregon, USA).

Photothermal evaluations of Na_xWO_3 nanoparticles
Photothermal performance was measured and analyzed by illuminating the cuvette containing different concentrations of Na_xWO_3 nanoparticles using a 980-nm wavelength laser with several different power intensity. One milliliter of Na_xWO_3 nanoparticles at different concentrations (0, 0.25,

0.5, 1 mg/mL) were illuminated by a 980-nm laser for 5 mins. One milliliter of Na_xWO_3 nanoparticles (1 mg/mL) solution was irradiated at various of power density (0.5, 1, 1.5, 2 W/cm^2) for 5 mins. In order to evaluate the stability of the photothermal performance of Na_xWO_3 nanoparticles, four cycles of heating (980 nm laser, 1 W/cm^2, 5 mins) and cooling periods (without laser irradiation) were performed. The temperature changes during all experiments were monitored by a photothermal camera (FLIRTM A325SC camera).

Cell ablation experiment

293T cells, murine breast cancer 4T1 cells and RAW264.7 cells were purchased from American Type Culture Collection (ATCC,Manassas, VA, USA) and cultured under standard conditions (37°C, 5% CO_2). To test the cytoxicity of Na_xWO_3 nanoparticles, 293T cells in 96-well plates were incubated with various concentrations of Na_xWO_3 nanoparticles (0, 12.5, 25, 50, 100, 200 mg/mL) for 24 or 48 hrs, after that, the MTT assay was carried out to determine the relative cell viabilities.

To test the photothermal cell ablation effectivity of Na_xWO_3 nanoparticles, 4T1 cells in 96-well plates were incubated with various concentrations of Na_xWO_3 nanoparticles (0, 12.5, 25, 50, 100, 200 mg/mL). After 4 hrs of incubation, the cells were irradiated by 980-nm laser at a power density of 1.5 W/cm^2 for 5 mins. After another 24 hrs of incubation, the MTT assay was carried out to determine the relative cell viabilities compared with the untreated group.

Subcutaneous 4T1 tumor ablation experiment

To develop the tumor model, 1×10^6 4T1 cells suspended in 100 μL PBS were subcutaneously injected into the back of each mouse. After 1 week, the average tumor sizes would reach to about 60 mm^3. For in vivo PTT, 4T1 tumor-bearing mice were randomly divided into four treatment groups: the first group was intravenously injected with saline solution (100 μL); the second group was exposed to 980-nm laser with a power density of 1.5 W/cm^2 for 8 hrs after injection with saline solution; the third group was intravenously injected with Na_xWO_3 nanoparticles (20 mg/kg) without NIR laser irradiation; and the fourth group was exposed to 980-nm laser with an output power density of 1.5 W/cm^2 for 5 mins at 8 hrs after intravenous injection of Na_xWO_3 nanoparticles (20 mg/kg). Tumor temperature and thermal images were visualized and recorded using the FLIRTM E50 camera. Hematoxylin-eosin (H&E) staining was

performed after treatments to compare the therapeutic efficacy of different treatment groups. The tumor volumes and body weights after treatments were recorded every 3 days for 2 weeks using caliper measurements and analytical balance. (The tumor volume was measured using the following equation ($V = L \times W^2 / 2$, in which L means the length of tumor and W means the width of tumor).)

Biodistribution test

Female nude mice were purchased from Nanjing Peng Sheng Biological Technology Co, Ltd (Peng Sheng Biological Technology Co, Ltd, Nanjing, China). Animal experiments were carried out following animal ethics. For biodistribution test, 100 μL of Na_xWO_3 nanoparticles (20 mg/kg) in PBS was intravenously injected into subcutaneous 4T1 tumor-bearing nude mice (n=9). Three main organs and tumor were obtained and dissolved by aqua regia at various time points (4, 8, 12 hrs) post-injection. To calculate the percentage of injected dose per gram of tissue (%ID/g) values in mouse organs and tumors, concentration of W was measured by inductively coupled plasma.

4T1 bone metastasis tumor ablation experiment

The Animal Care Committee of Central South University reviewed and approved all the animal care protocols and experimental procedures in this study. All animal experiments were conducted in accordance with the guiding principles of the Animal Care Committee of Central South University. A total of 20 BALB/c-nu/nu mice (4 weeks old, female) were purchased Shanghai Laboratory Animal Company, CAS (SLACCAS, Shanghai, China) and nurtured in specific pathogen-free (SPF) plastic-isolator cages and maintained in SPF laboratory animal facilities of Shanghai Lab, Animal Research Center. After acclimating to the facility for 7 days, all mice were anesthetized with 1% pentobarbital sodium. Subsequently, mice were subjected to an injection of 100 μL resuspended 4T1 cells at a density of 10^7 cells/mL in the tibiae plateau using a percutaneous approach to establish the breast cancer bone metastasis model. Two weeks later, after establishment of noticeable 4T1 breast cancer tissues in tibiae, the mice were randomly divided into four group; control group (0.9% NaCl), PTT group, Na_xWO_3 group (10 mg/kg nanoparticles), and Na_xWO_3+ PTT group (10 mg/kg nanoparticles). The second injection of nanoparticles and PTT were performed at 4th week. Body weight and tumor volume were recorded every 2 weeks. The tumor volume was measured

using the following equation ($V=0.2618 \times L \times W \times (L + W)$), where W: the average distance in the proximal tibia at the level of the knee joint in the anterior-posterior and medial-lateral planes; and L: the distance from the edge of the proximal of the tumor to the distal extent of tumor[4,31]).

μCT analysis

Six weeks after 4T1 injection, all mice were sacrificed for μCT scanning to evaluate cancer-associated osteolysis after treatments. The harvested tibiae were fixed in 4% paraformaldehyde. A three-dimensional reconstruction of breast cancer-bearing knee joint and quantitative bone volume fractions (BV/TV) was acquired as previously described.[32–35]

Western blot

Murine breast cancer 4T1 cells were administered with different treatments, respectively. Afterward, total proteins of cells were harvested under radioimmunoprecipitation assay (RIPA) lysis buffer containing phenylmethylsulfonyl fluoride. Western blot experiments for Bax, p-Akt, Sclerostin, RANKL and Sclerostin were performed based on previous reports with antibodies purchased from Abcam/Cell signaling Technology (Abcam, Shanghai, China and CST, Danvers, MA, USA).

TRAP staining after CM treatments

After treatments against 4T1 cells by PTT, Na_xWO_3 and Na_xWO_3+ PTT, conditioned medium (CM) from breast cancer cells were collected. Next, relative CM was used to administer osteoclast precursor RAW 264.7 cells.

RAW 264.7 cells seeded in 96-well plates were administered with different CM treatments and 50 ng/mL RANKL, respectively, for 7 days. After the maturation of RAW 264.7 cells, 4% paraformaldehyde (PFA) was used to fix the cells followed by the complete rinse of PBS. Next, the tartrate-resistant acid phosphatase (TRAP) staining was used to label the matured multi-nucleated osteoclasts, among which the stained osteoclast with at least three nuclei was classified as TRAP-positive osteoclasts.[36]

Statistical analysis

One-way ANOVA was used to determine the significance among groups. All values are expressed as mean ± SD. P-value ≤0.05 was considered statistically significant.

Result and discussion

The size and morphology of Na_xWO_3 nanoparticles were investigated using TEM, as shown in Figure 1A and B, the nanocrystals were cube-like and about 150–200 nm in length.

In addition, as the high-resolution TEM (Figure 1C) shown, clear lattice fringe indicating the good crystallinity of Na_xWO_3 nanoparticles. The XRD was also performed, as demonstrated in Figure 1D, all peaks were well matched with Na_xWO_3 phase indicating the successful preparation of Na_xWO_3 nanoparticles.

Next, we evaluated the photothermal performance of Na_xWO_3 nanoparticles in vitro. As the UV-vis-NIR absorbance of Na_xWO_3 nanoparticles solution (Figure 2A) indicated, the absorption of Na_xWO_3 nanoparticles solution increasing obviously from 650 to 1000 nm. After that, the photothermal experiments were carried out. Different concentrations of Na_xWO_3 nanoparticles solution was irradiated under 980-nm laser for 5 mins at power intensity of 1 W/cm^2, the temperature of higher concentration (1 mg/mL) of Na_xWO_3 nanoparticles solution exhibited sharply increased from 25.8°C to 41.8°C in 5 mins. However, temperature of pure water sample was exhibited limited increase (Figure 2B and C). In addition, Na_xWO_3 nanoparticles solution (1 mg/mL) was irradiated under 980-nm laser for 5 mins at different power intensity (0.5, 1, 1.5, 2 W/cm^2), as shown in Figure 2D and E, the photothermal performance of Na_xWO_3 nanoparticles was heightened along with the increasing of laser power intensity. Beyond that, the photothermal stability of Na_xWO_3 nanoparticles was also monitored. As temperature profile showed in Figure 2F, no distinct recession could be found during the four cycles, which indicates the good photothermal stability of Na_xWO_3 nanoparticles.

Encouraged by the good photothermal ability of Na_xWO_3 nanoparticles, we tested its cytotoxicity and ablation efficient further. As shown in Figure 3A, after 24 or 48 hrs co-incubated with various concentrations (0, 12.5, 25, 50, 100, 200 mg/mL) Na_xWO_3 nanoparticles, negligible 293T cells death were observed, which indicated tiny cytotoxicity of Na_xWO_3 nanoparticles. Next, we test photothermal ablation efficient to 4T1 cells. As shown in Figure 3B, 4T1 cells were then treated with 980-nm laser (1.5 W/cm^2, 5 mins) of various concentrations of Na_xWO_3 nanoparticles (0, 12.5, 25, 50, 100, 200 mg/mL). It was found that the relative viabilities of the 4T1 cells decreased remarkably at elevated Na_xWO_3 concentration. In contrast, negligible cell killing was found for the groups without any treatment or treatment with NIR laser only.

The good tumor cells ablation result encouraged us for applying it to in vivo tumor therapy. Before tumor therapy, it is necessary to know the bio-distribution of Na_xWO_3 nanoparticles concentration in mice so as to confirm suitable time point for PTT. As shown in Figure 4A, an obvious gathering of Na_xWO_3 was detected after 4 hrs intravenous injection
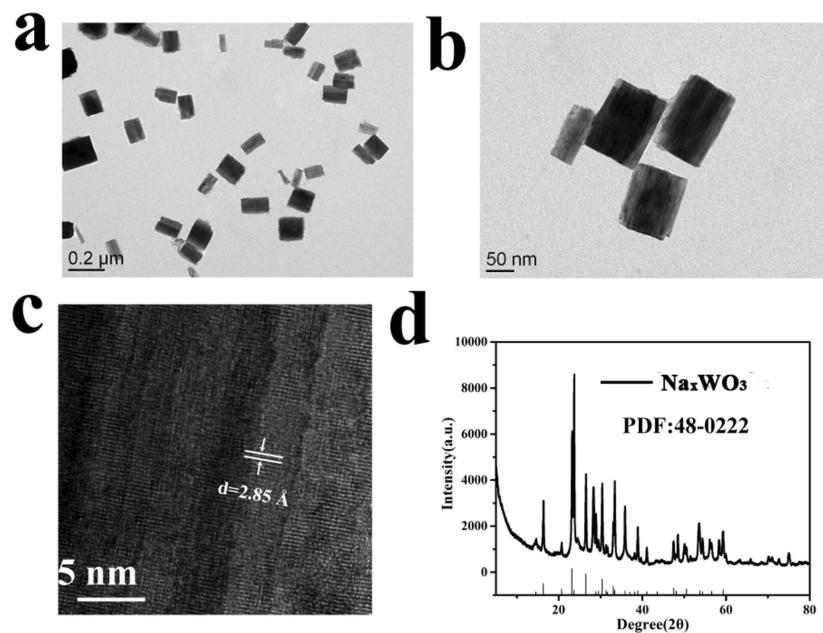
Figure 1 (**A**) and (**B**) TEM images of Na_xWO_3 nanoparticles. (**C**) High-resolution TEM image of a Na_xWO_3 nanoparticle. (**D**) XRD pattern of Na_xWO_3 nanoparticles.
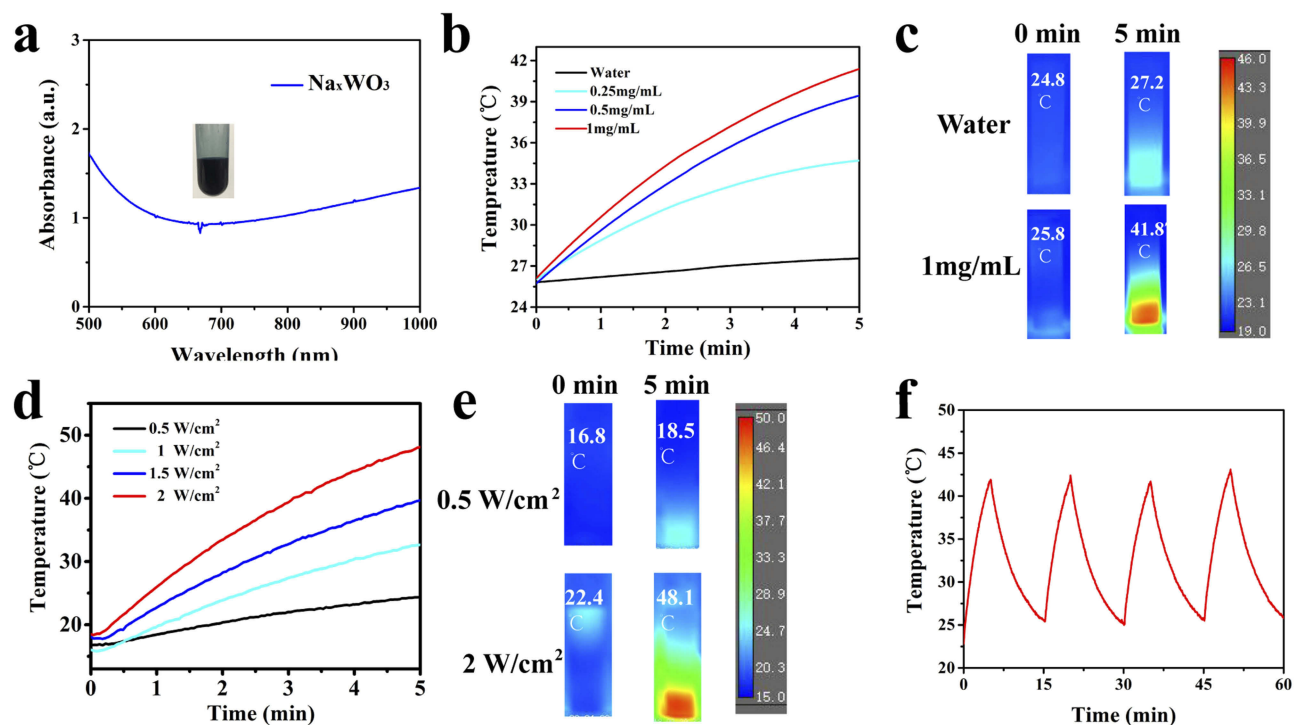**Abbreviations:** TEM, transmission electron microscopy; XRD, X-ray diffraction.

Figure 2 (**A**) UV-Vis-NIR absorbance of Na_xWO_3 nanoparticles solution (200 μg/mL), photograph of Na_xWO_3 nanoparticles solution was shown in the insert. (**B**) Temperature increase curves of a Na_xWO_3 nanoparticles solution under an 980 nm-wavelength laser irradiation at various concentrations (0, 0.25, 0.5, 1 mg/mL) at a power intensity of 1 W/cm^2 for 5 mins. (**C**) Representative thermal images of water or Na_xWO_3 nanoparticles solution (1 mg/mL) under 980 nm-wavelength laser irradiation at a power intensity of 1 W/cm^2. (**D**) Temperature increase curves of Na_xWO_3 nanoparticles solution (1 mg/mL) under various power intensity (0.5, 1, 1.5, 2 W/cm^2) of 980 nm-wavelength laser for 5 mins. (**E**) Representative thermal images of Na_xWO_3 nanoparticles solution (1 mg/mL) under 980 nm-wavelength laser irradiation at a power intensity of 0.5 W/cm^2 or of 2 W/cm^2. (**F**) Four heating and cooling cycles of Na_xWO_3 nanoparticles solution (1 mg/mL) (980 nm laser, 1 W/cm^2).
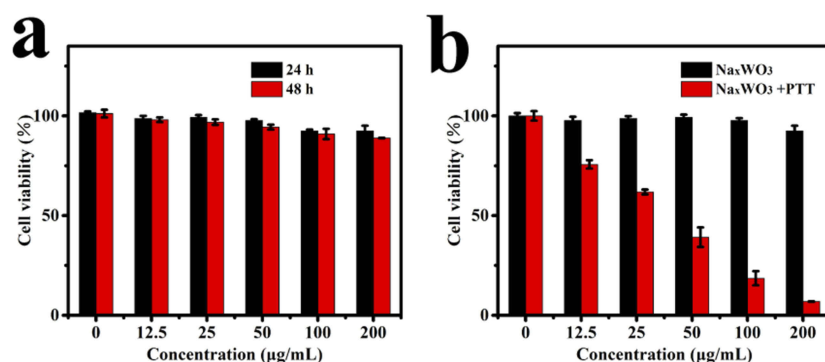**Abbreviation:** NIR, near-infrared.

Figure 3 (**A**) Relative viabilities of 293T cells after they were incubated for 24 and 48 hrs with Na_xWO_3 nanoparticles of various concentrations (0, 12.5, 25, 50, 100, 200 mg/mL) (n=5, mean ± s.d.). (**B**) Inhibition of the growth of 4T1 cells incubated with Na_xWO_3 nanoparticles of various concentrations (0, 12.5, 25, 50, 100, 200 mg/mL) and then irradiated with 980 nm-wavelength lasers (1.5 W $cm^{/2}$) for 5 mins (n=5, mean ± s.d.).
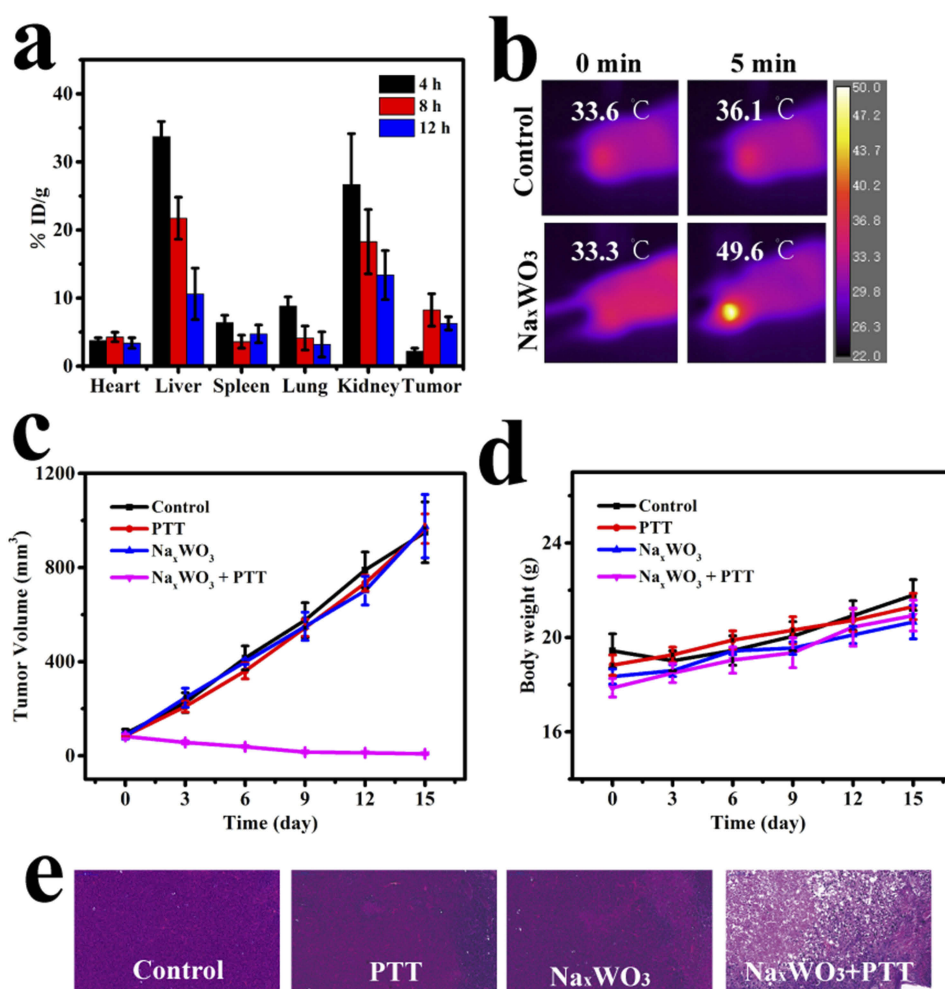**Abbreviation:** PTT, photothermal therapy.

Figure 4 (**A**) Biodistribution profile of Na_xWO_3 nanoparticles in 4T1 tumor-bearing mice at various time intervals (4, 8, and 12 hrs) after the i.v. injection of Na_xWO_3 nanoparticles, as determined by measuring W in homogenized tissue solutions (n=3, mean ± s.d.). (**B**) Representative thermal images of bilateral 4T1 tumor-bearing mice that were irradiated with a 980 nm-wavelength laser (1.5 W $cm^{/2}$) 8 hrs after injection with saline or Na_xWO_3 nanoparticles (20 mg/kg). (**C**) Time-dependent change of relative tumor volume after various treatments (n=5, mean ± s.d.). (**D**) Time-dependent change of mice body weight after various treatments (n=5, mean ± s.d.). (**E**) Representative images of H&E-stained tumor sections of various groups (control, control + 980 nm-wavelength laser, Na_xWO_3, Na_xWO_3 980 nm-wavelength laser).
Abbreviation: PTT, photothermal therapy.

owing to enhanced permeability effect (EPR), and reached to a peak level in 8 hrs. Therefore, 8 hrs tail vein post-injection was selected for PTT experiments.

After that, in vivo 4T1 tumor PTT was carried out. The tumor temperature and thermal images were visualized with a thermal camera. As shown in Figure 4B, the temperature of the tumor rapidly increased to above 49.6°C in 5 mins under 980-nm laser irradiation (1.5 W/cm^2), which was sufficient to thermally ablate the tumor, while the control group (without Na$_x$WO$_3$ nanoparticles injection) showed only limited temperature increase. For the treated group, 4T1 tumor growth was eliminated (Figure 4C), whereas the control groups demonstrated rapid tumor growth. Hematoxylin and eosin (H&E) staining of tumors from different groups further confirmed the above results, where the treatment group shows the most tumor damage (Figure 4E). No abnormal behavior or significant weight loss was observed in any group (Figure 4D), indicating minimal side effects of Na$_x$WO$_3$ nanoparticles.

On the basis of excellent PTT performance and previous in vitro inhibitory effect and in vivo percutaneous 4T1 breast cancer model of Na$_x$WO$_3$ nanoparticles, we hypothesized that Na$_x$WO$_3$ nanoparticles could also prevent breast cancer bone establishment in vivo. Herein, we constructed a breast cancer bone metastasis model by the injection of 4T1 breast cancer cells intratibially. In the control group and PTT group, as shown in Figure 5A, severe osteolytic bone lesions and destruction of cortices were observed. In contrast, there were fewer osteolytic lesions in the Na$_x$WO$_3$ group, and the cortices remained intact. Such bone protective effect was more obvious in Na$_x$WO$_3$+PTT group. Quantitative analysis of the bone parameters confirmed these results, as evidenced by a significant increase in BV/TV (Figure 5B). In addition, despite that there was no significant difference in the body weight of four groups during observation (Figure 5C), mice treated with Na$_x$WO$_3$+ PTT resulted in a significant decrease of tumor volume (Figure 5D), indicating the significant biosafety as well as tumor ablation abilities of Na$_x$WO$_3$ nanoparticles simultaneously.

More interestingly, we also found that both the Bax (pro-apoptotic protein) and p-Akt levels in 4T1 breast cancer cells were increased after Na$_x$WO$_3$+PTT treatment, regardless of the similar tendency in PTT and Na$_x$WO$_3$ group compared with control group. These results indicated that Na$_x$WO$_3$+PTT treatments facilitated the breast cancer cells apoptosis by augmenting the Bax and phosphorylated Akt expressions. Importantly, both osteoclastic stimulus RANKL and Sclerostin expressions were significantly decreased after Na$_x$WO$_3$+PTT treatments compared with individual treatment
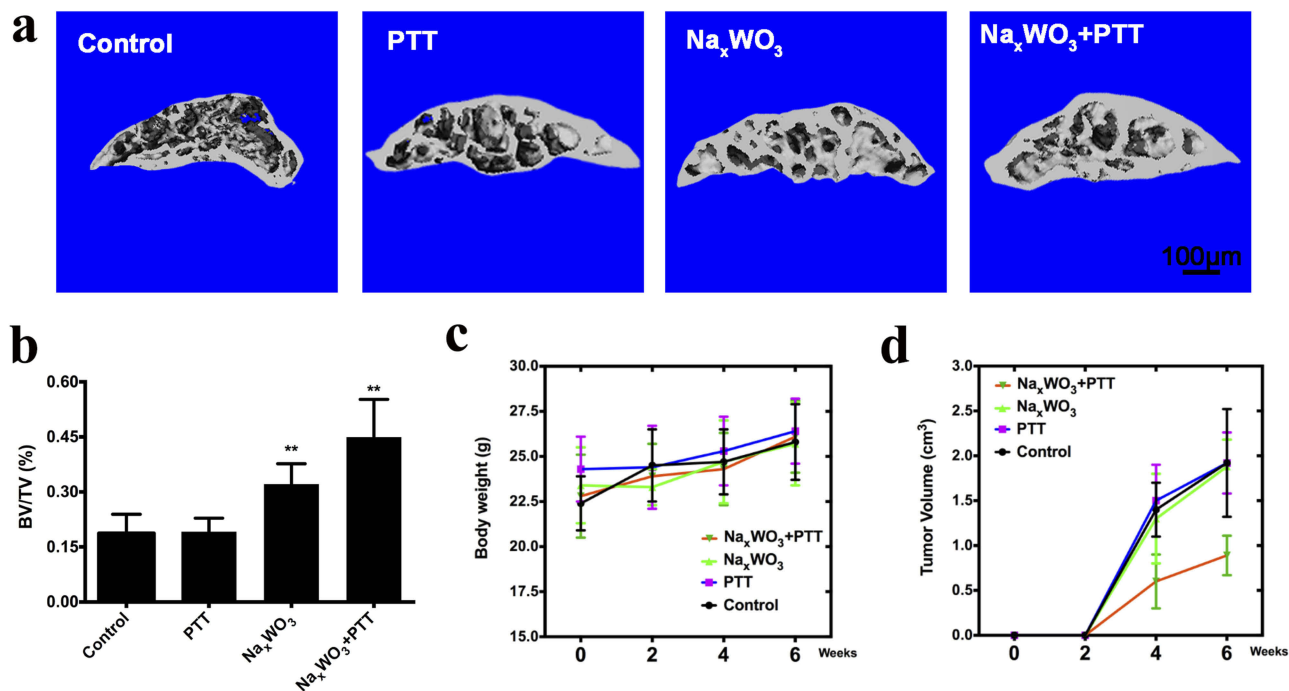

Figure 5 (**A**) Representative images of µCT of the tibia trabecular bone medial compartment treated with 0.9% sodium chloride (control group), PTT (PTT group), NaxWO3 (NaxWO3 group), and NaxWO$_3$+PTT (NaxWO$_3$+PTT group). Scale bar, 100 µM. (**B**) Bone volume/tissue volume (BV/TV) was measured by quantitative analysis of µCT. The significance was determined as indicated in methods (**$P<0.01$ versus control). (**C**) Evaluation of cachexia by body weight that was recorded every 2 weeks until 6th week. (**D**) Quantitation of tumor volume of mice in each group.
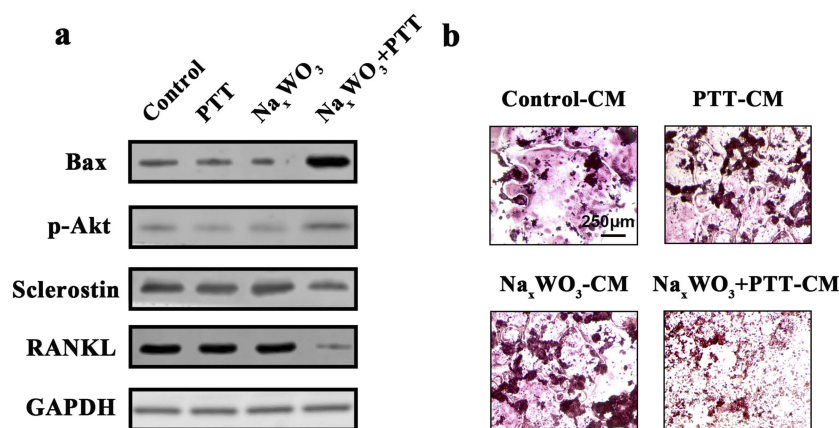**Abbreviation:** PTT, photothermal therapy.

Figure 6 (**A**) Proteins expressions for Bax, p-Akt, Sclerostin and RANKL in 4T1 cells. (**B**) Osteoclastogenesis of RAW 264.7 cells at 7th day after stimulations by CM from 4T1 cells treated with control, PTT, Na_xWO_3, and Na_xWO_3+PTT. Scale bar, 250 μM.
Abbreviations: PTT, photothermal therapy; CM, conditioned medium.

and control group, signifying that Na_xWO_3+PTT treatments could attenuate the release of osteoclastic factors from breast cancer 4T1 cells (Figure 6A). Hence, we collected the CM from 4T1 cells to further administer osteoclastic RAW 264.7 cells. Figure 6B shows that in control-CM group, large and red-stained matured osteoclasts were formed together with PTT-CM and Na_xWO_3-CM groups. Nonetheless, in Na_xWO_3+PTT group, less and smaller osteoclasts were stained by TRAP solution, indicating the significant inhibition by Na_xWO_3+PTT treatments against 4T1 cells to induce subsequent osteoclast formation. Based on the above WB results, this could be ascribed from the reduced RANKL and Sclerostin secretion from 4T1 cells after Na_xWO_3+PTT treatments. Collectively, our results indicated that Na_xWO_3+PTT could prevent bone destruction of breast cancer and inhibit tumor growth significantly both in vitro and in vivo.

Conclusion

Herein, for the first time, we developed a novel oxygen vacancy-rich tungsten bronze nanoparticles (Na_xWO_3) through a simple pyrogenic decomposition process for PTT. As the results indicated, Na_xWO_3 nanoparticles showed excellent photothermal conversion ability and photothermal stability in vitro. In addition, percutaneous 4T1 tumor was eliminated without recurrence during 2 weeks observation after Na_xWO_3+PTT administration. More importantly, intratibial breast cancer model confirmed the desirable PTT effects of novel Na_xWO_3 nanoparticles against 4T1 breast cancer cells, showing decreased bone destruction as well as tumor volume in vivo. Mechanistic studies showed that Na_xWO_3 +PTT treatments increased apoptotic Bax and p-Akt expressions. More importantly, Na_xWO_3+PTT treatments inhibited

the osteoclastic RANKL and Sclerostin expressions from 4T1 cells, therefore further attenuated downstream osteoclastogenesis. Therefore, our novel PTT strategy of Na_xWO_3 could provide brand-new insight into future cancer bone metastasis treatment clinically, which also expand the research horizons of PTT nanomaterials.

Disclosure

The authors report no conflicts of interest in this work.

References

1. Lin Z, Liu Y, Ma X, et al. Photothermal ablation of bone metastasis of breast cancer using PEGylated multi-walled carbon nanotubes. *Sci Rep*. 2015;5:11709. doi:10.1038/srep11709
2. Fan L, Strasser-Weippl K, Li J-J, et al. Breast cancer in China. *Lancet Oncol*. 2014;15(7):e279–e289. doi:10.1016/S1470-2045(13)70567-9
3. Croset M, Goehrig D, Frackowiak A, et al. TWIST1 expression in breast cancer cells facilitates bone metastasis formation. *J Bone Miner Res*. 2014;29(8):1886–1899. doi:10.1002/jbmr.2215
4. Yuan G, Lian Z, Liu Q, et al. Phosphatidyl inositol 3-kinase (PI3K)-mTOR inhibitor PKI-402 inhibits breast cancer induced osteolysis. *Cancer Lett*. 2019;443:135–144. doi:10.1016/j.canlet.2018.11.038
5. Steenbruggen TG, van Ramshorst MS, Kok M, Linn SC, Smorenburg CH, Sonke GS. Neoadjuvant therapy for breast cancer: established concepts and emerging strategies. *Drugs*. 2017;77(12):1313–1336. doi:10.1007/s40265-017-0774-5
6. Woo SB, Solomon DH. Bisphosphonate therapy for cancer and prevalence of inflammatory jaw conditions. *J Natl Cancer Inst*. 2007;99 (13):986–987. doi:10.1093/jnci/djm029
7. Josse R, Khan A, Ngui D, Shapiro M. Denosumab, a new pharmacotherapy option for postmenopausal osteoporosis. *Curr Med Res Opin*. 2013;29(3):205–216. doi:10.1185/03007995.2013.763779

8. Jiang M, Yan Y, Yang K, et al. Small molecule nAS-E targeting cAMP response element binding protein (CREB) and CREB-binding protein interaction inhibits breast cancer bone metastasis. *J Cell Mol Med*. 2019;23(2):1224–1234. doi:10.1111/jcmm.14024

9. Eyvazzadeh N, Shakeri-Zadeh A, Fekrazad R, Amini E, Ghaznavi H, Kamran Kamrava S. Gold-coated magnetic nanoparticle as a nanotheranostic agent for magnetic resonance imaging and photo-thermal therapy of cancer. *Lasers Med Sci*. 2017;32(7):1469–1477. doi:10.1007/s10103-017-2267-x

10. Mirrahimi M, Abed Z, Beik J, et al. A thermo-responsive alginate nanogel platform co-loaded with gold nanoparticles and cisplatin for combined cancer chemo-photothermal therapy. *Pharmacol Res*. 2019;143:178–185. doi:10.1016/j.phrs.2019.01.005

11. Hauck TS, Jennings TL, Yatsenko T, Kumaradas JC, Chan WCW. Enhancing the toxicity of cancer chemotherapeutics with gold nanorod hyperthermia. *Adv Mater*. 2010;20(20):3832–3838. doi:10.1002/adma.v20:20

12. Dong K, Liu Z, Li Z, Ren J, Qu X. Hydrophobic anticancer drug delivery by a 980 nm laser-driven photothermal vehicle for efficient synergistic therapy of cancer cells in vivo. *Adv Mater*. 2013;25 (32):4452–4458. doi:10.1002/adma.201301232

13. Huang P, Lin J, Li W, et al. Biodegradable gold nanovesicles with an ultrastrong plasmonic coupling effect for photoacoustic imaging and photothermal therapy. *Angew Chem Int Ed*. 2013;125(52):13958–13964. doi:10.1002/anie.201308986

14. Lal S, Clare SE, Halas NJ. Nanoshell-enabled photothermal cancer therapy: impending clinical impact. *Acc Chem Res*. 2008;41(12):1842–1851. doi:10.1021/ar800150g

15. O'Neal DP, Hirsch LR, Halas NJ, Payne JD, West JL. Photo-thermal tumor ablation in mice using near infrared-absorbing nanoparticles. *Cancer Lett*. 2004;209(2):171–176. doi:10.1016/j.canlet.2004.02.004

16. Huang X, El-Sayed IH, Qian W, El-Sayed MA. Cancer cell imaging and photothermal therapy in the near-infrared region by using gold nanorods. *J Am Chem Soc*. 2006;128(6):2115–2120. doi:10.1021/ja057254a

17. Alamzadeh Z, Beik J, Pirhajati Mahabadi V, et al. Ultrastructural and optical characteristics of cancer cells treated by a nanotechnology based chemo-photothermal therapy method. *J Photochem Photobiol B*. 2019;192:19. doi:10.1016/j.jphotobiol.2019.01.005

18. Beik J, Khademi S, Attaran N, et al. A nanotechnology based strategy to increase the efficiency of cancer diagnosis and therapy: folate conjugated gold nanoparticles. *Curr Med Chem*. 2017;24(39):4399–4416.

19. Beik J, Khateri M, Khosravi Z, et al. Gold nanoparticles in combinatorial cancer therapy strategies. *Coord Chem Rev*. 2019;387:299–324. doi:10.1016/j.ccr.2019.02.025

20. Ghaznavi H, Hosseini-Nami S, Kamrava SK, et al. Folic acid conjugated PEG coated gold–iron oxide core–shell nanocomplex as a potential agent for targeted photothermal therapy of cancer. *Artif Cells Nanomed Biotechnol*. 2017;46(8):1–11. doi:10.1080/21691401.2017.1384384

21. Mirrahimi M, Hosseini V, Kamrava SK, et al. Selective heat generation in cancer cells using a combination of 808 nm laser irradiation and the folate-conjugated Fe2O3@Au nanocomplex. *Artif Cell*. 2018;46(sup1):241–253.

22. Liu T, Wang C, Gu X, et al. Drug delivery with PEGylated MoS_2 nano-sheets for combined photothermal and chemotherapy of cancer. *Adv Mater*. 2014;26(21):3433–3440. doi:10.1002/adma.201305256

23. Song XR, Wang X, Yu S-X, et al. Co9Se8 nanoplates as a new theranostic platform for photoacoustic/magnetic resonance Dual-Modal-Imaging-Guided Chemo-Photothermal combination therapy. *Adv Mater*. 2015;27(21):3285–3291. doi:10.1002/adma.201405634

24. Yong Y, Cheng X, Bao T, et al. Tungsten sulfide quantum dots as multifunctional nanotheranostics for in vivo dual-modal image-guided photothermal/radiotherapy synergistic therapy. *ACS Nano*. 2015;9(12):12451–12463. doi:10.1021/acsnano.5b05825

25. Liu Z, Chen K, Davis C, et al. Drug delivery with carbon nanotubes for in vivo cancer treatment. *Cancer Res*. 2008;68(16):6652. doi:10.1158/0008-5472.CAN-07-5873

26. Yang K, Zhang S, Zhang G, et al. Graphene in mice: ultrahigh in vivo tumor uptake and efficient photothermal therapy. *Nano Lett*. 2010;10 (9):3318. doi:10.1021/nl1017157

27. Cong S, Yuan Y, Chen Z, et al. Noble metal-comparable SERS enhancement from semiconducting metal oxides by making oxygen vacancies. *Nat Commun*. 2015;6(6, 7):7800. doi:10.1038/ncomms8800

28. Gordon TR, Cargnello M, Paik T, et al. Nonaqueous synthesis of TiO_2 nanocrystals using TiF_4 to engineer morphology, oxygen vacancy concentration, and photocatalytic activity. *J Am Chem Soc*. 2012;134(15):6751–6761. doi:10.1021/ja300823a

29. Xi G, Ouyang S, Li P, et al. Ultrathin W 18 O 49 nanowires with diameters below 1 nm: synthesis, near-infrared absorption, photoluminescence, and photochemical reduction of carbon dioxide. *Angew Chem Int Ed*. 2012;51(10):2395–2399. doi:10.1002/anie.201107681

30. Huang Q, Hu S, Zhuang J, Wang X. MoO_{3-x}-based hybrids with tunable localized surface plasmon resonances: chemical oxidation driving transformation from ultrathin nanosheets to nanotubes. *Chemistry*. 2012;18(48):15283–15287. doi:10.1002/chem.201202630

31. Ouyang Z, Wang S, Zeng M, et al. Therapeutic effect of palbociclib in chondrosarcoma: implication of cyclin-dependent kinase 4 as a potential target. *Cell Commun Signal*. 2019;17(1):17. doi:10.1186/s12964-019-0327-5

32. Ouyang Z, Guo X, Chen X, et al. Hypericin targets osteoclast and prevents breast cancer-induced bone metastasis via NFATc1 signaling pathway. *Oncotarget*. 2018;9(2):1868–1884. doi:10.18632/oncotarget.22930

33. Zhu W, Yin Z, Zhang Q, et al. Proanthocyanidins inhibit osteoclast formation and function by inhibiting the NF-kappaB and JNK signaling pathways during osteoporosis treatment. *Biochem Biophys Res Commun*. 2019;509(1):294–300. doi:10.1016/j.bbrc.2018.12.125

34. Ouyang Z, Tan T, Liu C, et al. Targeted delivery of hesperetin to cartilage attenuates osteoarthritis by bimodal imaging with Gd2 (CO3)3@PDA nanoparticles via TLR-2/NF-κB/Akt signaling. *Biomaterials*. 2019;205:50–63. doi:10.1016/j.biomaterials.2019.03.018

35. Zhang Q, Tang X, Liu Z, et al. Hesperetin prevents bone resorption by inhibiting RANKL-induced osteoclastogenesis and Jnk mediated Irf-3/c-Jun activation. *Front Pharmacol*. 2018;9:1028. doi:10.3389/fphar.2018.01028

36. Ouyang Z, Huang Q, Liu B, et al. Rubidium chloride targets Jnk/p38-mediated NF-kappaB activation to attenuate osteoclastogenesis and facilitate osteoblastogenesis. *Front Pharmacol*. 2019;10:584. doi:10.3389/fphar.2019.00848